Light Pipe for High Intensity Laser Pulses

C. G. Durfee III and H. M. Milchberg

Institute for Physical Science and Technology and Department of Electrical Engineering, University of Maryland,
College Park, Maryland 20742

Optical guiding of intense laser pulses over a distance of more than 20 Rayleigh lengths in a plasma is demonstrated using a two-pulse technique. The first pulse prepares a shock-driven, axially extended radial electron density profile which guides a second pulse, injected after an optimum delay which increases with mass of the plasma ions. In the intensity range considered here (10^{13}–10^{14} W/cm^2), the channel is observed to support mode structure reminiscent of an optical waveguide.

PACS numbers: 52.40.Nk, 52.35.Mw, 52.40.Db

We demonstrate for the first time the optical guiding of a high intensity laser pulse over distances well in excess of a Rayleigh length, using a prepared plasma refractive index channel. The distance over which guiding occurs appears to be limited only by the length of the preformed plasma and absorption and possible backscattering of the guided pulse. We describe two experiments. The first is a proof-of-principle demonstration of the channeling effect using two pulses, one following the other with variable delay, focused by the same lens. In this experiment, the plasma channel, with an electron density minimum on axis, is generated by the hydrodynamic evolution of the breakdown spark created by the first pulse. The channel is slightly longer than a confocal parameter. The second pulse, injected after an appropriate delay, experiences lensing due to this short channel. In the second experiment, we extend the channel to 0.7 cm (24 Rayleigh lengths) by means of an axicon [1]. After an optimum delay, the second pulse is injected into the end of the channel from the opposite direction. The beam is observed to be confined over the length of the channel, at intensities of up to 10^{14} W/cm^2 for the conditions explored here.

There has been a resurgence of interest in channeling high-intensity laser pulses through plasmas over distances exceeding a Rayleigh length. An early proposed application for channeling was nuclear fusion [2] using long pulse or cw lasers. Recent suggested applications, using intense short pulses, include pumping of x-ray lasers [3] and laser-plasma-based particle accelerators [4]. Experiments involving nonlinear processes, such as high harmonic generation [5], may also benefit from an increased interaction length.

One approach to channeling of intense pulses, suggested by recent advances in intense pulse laser technology [6], relies on self-induced modifications of the plasma refractive index. The on-axis enhancement of refractive index by relativistic electron dynamics or by ponderomotive force-driven charge displacement [7] requires extremely high intensities (above 10^{18} W/cm^2). Recent calculations show that such an intense short pulse is subject to erosion: The leading edge diffracts due to a balance between forward charge displacement and relativistic electron response [8] and the trailing edge is scattered by Raman instabilities [9]. Even more fundamentally, it is not clear that such focused intensities can even be achieved in a medium: Beams approaching the focus can refract due to plasma formation [10] or undergo filamentation [11] at much lower thresholds than the onset of charge displacement or relativistic effects. The use of prepared index structures, however, provides a means of *stable* channeling, as we will demonstrate.

Previous work has demonstrated that laser-produced sparks in gases can produce plasma density minima on axis. Reduced scattering has been observed for electron beams injected into 3 J, 30 ns pulse laser-produced sparks [12]. On-axis density minima have also been observed in the interaction of 150 ns CO_2 laser pulses with helium at 30 torr, where refraction of the unstable resonator mode was interpreted as evidence for self-focusing [13].

As a guide for our experiments, and to understand in detail how favorable refractive index profiles are generated, we have performed calculations of gas response to irradiation by intense pulses. The model includes tunneling ionization in the laser field [14] [as an approximation to multiphoton ionization (MPI)], laser-plasma heating via inverse bremsstrahlung, thermal conduction, and collision-based ionization and recombination. Figure 1 shows calculations of radial electron density profiles generated in 30 torr of Ar as a function of time for a 100 ps, 4×10^{14} W/cm^2 peak intensity pulse. A general picture of the plasma dynamics can be deduced from these calculations: At lower pressures (< 50 torr), ionization during the laser pulse is mostly attributable to direct ionization by the laser field while the electrons are heated by inverse bremsstrahlung (in Fig. 1 to a maximum of ~ 120 eV). Collisional ionization takes place after the laser pulse, on the time scale of a few nanoseconds, so that the plasma is strongly out of equilibrium. At higher pressures, depending on the gas, avalanche ionization contributes more significantly to the breakdown. The ion temperature remains small over many nanoseconds due to weak electron-ion coupling. Since the tunneling rates increase strongly with laser field strength and space charge keeps the plasma electrically neutral, there is a well-defined boundary, with a precursor controlled by thermal conduction, between the heated plasma and the neutral or weakly ionized gas on the periphery. This results in a large
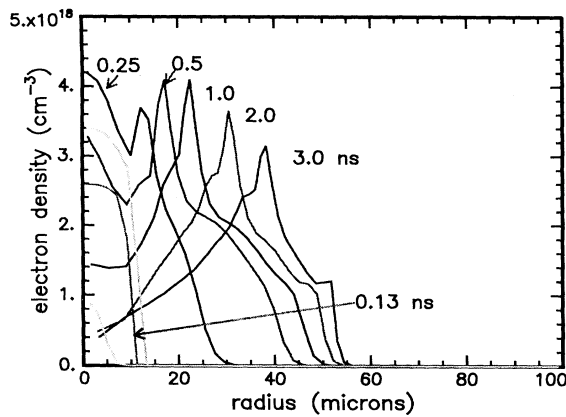
FIG. 1. Calculation of 30 torr Ar response to laser pulse of peak intensity $I = 4 \times 10^{14}$ W/cm^2, spot size $w_0 = 10$ μm, $\lambda = 1.064$ μm, $\tau_p = 100$ ps. The rapid rise of N_e at early times is due to direct ionization by the laser. The laser pulse, Gaussian in time, peaks at $t = 0.125$ ns.

FIG. 2. (a) Optical arrangement for first experiment. (b) Fluorescence images (CCD$_1$) from spark in 30 torr Ar with $E_1 = 70$ mJ, $E_2 = 70$ mJ, and $w_0 = 10$ μm for various delays of pulse 2. Lens L is to the left. (c) Probe (pulse 2) far-field patterns (CCD$_2$) for the same delays as (b).

pressure gradient which drives a shock wave in the ion density as the heated electrons move outward, pulling the relatively cold ions along at the local ion sound speed $c_s = (ZkT_e/m_i)^{1/2}$. A depression in the plasma density develops on axis behind the shock, yielding a refractive index profile which can focus a beam. Two time scales τ can be deduced from this plot: for shock evolution $\tau = $ (shock thickness)/(sound speed) ≈ 100 ps and for overall plasma evolution $\tau = $ (spot size)/(sound speed) ≈ 1 ns. The pulse duration ($\tau_p = 100$ ps) and the two-pulse delays (0–15 ns) used in our experiments are well suited to the plasma dynamics. Longer laser pulses [13] would continue to heat the plasma during the shock expansion phase, resulting in a much broader pressure profile and a very wide channel which would be less useful as an optical guide; much shorter pulses of equal energy would not heat the electrons sufficiently to drive the expansion in the presence of conduction losses, since for short pulses the plasma temperature increases scales as $\tau_p^{1/2}$. Using ponderomotive force charge displacement to generate the radial electron density variations of Fig. 1 would require intensities of at least 5×10^{18} W/cm^2.

In the first of our two experiments, we demonstrate that lensing of a laser pulse in ionized gases can be achieved by using two pulses: The first pulse forms a channel for the second. A mode-locked Nd:YAG laser provides 100 ps, $\lambda = 1.064$ μm seed pulses for input to a 10 Hz flashlamp-pumped Nd:YAG regenerative amplifier (RGA) system [15]. A beam splitter and delay line is placed at the input to the RGA, which results in two output pulses of adjustable relative energy and time separation (0–6 ns), and identical direction and spatial mode. The pulses are then double passed through a power amplifier, with final total pulse energy $E = E_1 + E_2$ of up to 250 mJ, and then focused at $f/10$ by a 250 mm focal length aplanatic lens (L) inside a chamber; see Fig. 2(a).
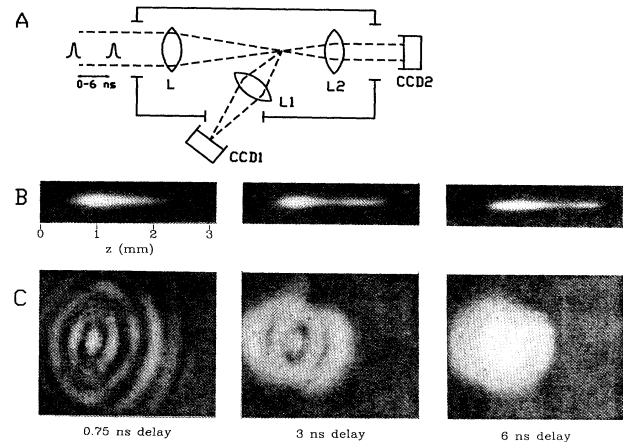
Lens L_1 imaged scattered laser light and recombination emission (which we call "fluorescence") from the focal region plasma to a charge-coupled-device camera (CCD$_1$). For laser scattering, a 3 nm bandpass filter around 1.064 μm was used, while an infrared blocking filter was used for fluorescence. An aplanatic lens L_2, on axis, collected laser light at $f/3$ for camera CCD$_2$. Here, images due to pulse 1 were subtracted from two-pulse images in order to provide a pump-probe record of diffraction and refraction of pulse 2 from the evolving plasma. For all images, the signal-to-noise ratio and resolution were improved by using 100 shot averages.

In Fig. 2(b), a sequence of spark fluorescence images (CCD$_1$) is shown for argon at 30 torr for different delays of pulse 2. Here, $E_1 = 70$ mJ and $E_2 = 70$ mJ (pulse peak intensity 4×10^{14} W/cm^2, spot size $w_0 = 10$ μm). Fluorescence shows similar spatial structure as laser scattering (which is weak at 30 torr), although more diffuse, since, unlike the prompt laser scattering, recombination emission occurs over tens of nanoseconds. As the delay of the second pulse is increased, the spark is lengthened in the direction away from the focusing lens. The onset of lengthening occurs at approximately 3 ns. For nitrogen and xenon, lengthening starts at about 1.3 ns and 5 ns for these conditions. This is in accord with the calculations, which show that heavier gases take longer to develop channels, due to the decrease in ion sound speed. At even longer delays, a secondary spark becomes more pronounced and separates from the first. This is explained in terms of a simple model for a Gaussian beam focused into a short channel with index profile $n = 1 - \frac{1}{2} N_e(r)/N_{cr}$, where N_{cr} is the plasma critical density, and $N_e(r)$ increases quadratically from $r = 0$. If the input beam is collimated at the channel entrance, guiding will occur at constant beam size if the electron density difference be-

tween $r=0$ and $r=w_0$ is $\Delta N_e \approx 1/\pi r_e w_0^2$, set by a balance between positive lensing by the plasma and diffraction over a Rayleigh length, where r_e is the classical electron radius. However, in this configuration the plasma is created by pulse 1 on both sides of the focus, and so pulse 2 is converging when it encounters the entrance to the channel. If the index curvature is large enough that the beam waist can complete more than one full period of oscillation, a second spark will appear beyond the original channel. For a given spot size, the maximum separation between the two spark maxima is a function of the length of the channel. For the measured channel length of 1.2 mm, the observed peak separation corresponds to $\Delta N_e \approx 10^{18}$ cm^{-3}, in agreement with the calculations of Fig. 1.

Figure 2(c) shows probe (pulse 2) far-field patterns (CCD$_2$), for the same delays as in Fig. 2(b). Here, the pulse energies were $E_1=70$ mJ and $E_2=10$ mJ. Increasing E_2 to 70 mJ changed the resulting images little. The plasmas are sufficiently long that the patterns result from both diffraction and refraction of the probe pulse. At 0.75 ns, large angle scattering (which overfilled L_2) indicates the presence of sharp spatial structure of size ~ 2 μm in the interaction region, consistent with a shock. At 3 ns, this large angle scattering is gone, while there is still modulation close to the beam center. It is at this delay that the probe beam fits inside the shock and lengthening of the spark begins, as seen in Fig. 2(b). By 6 ns, the lensing is still sufficient to cause an oscillation, but the beam profile modulation disappears.

The length of the plasma formed by the initial pulse clearly determines the extent to which a second pulse can be guided. In the second experiment we produce a long, uniform plasma by means of an axicon [1], which forms an extended focus along the optical axis. Here, we use a BK-7 glass cone ($n=1.51$ at 1.06 μm) with base angle $\alpha=35°$ and an axial hole of diameter $2a=3.2$ mm. The axicon directs rays from a collimated beam at angle $\gamma \approx 25°$ with respect to the optical axis. The axial hole allows passage of an oppositely directed beam. The field dependence near the axis is $|E(r,z)|^2=|E_0(z)|^2 J_0^2 \times (kr\sin\gamma)$, where $|E_0(z)|^2$ depends on the transverse field distribution of the incident beam and k is the laser wave number [16]. The axially extended focus is of length $L=(R-a)(1/\tan\gamma-\tan\alpha) \approx 1$ cm and radius $r_0=0.38\lambda/\sin\gamma \approx 1$ μm, where $R=0.79$ cm is the beam radius at the axicon input. We have observed uniform sparks of length ≈ 1 cm in both the MPI and avalanche regimes. Axicon-generated sparks have been produced in earlier work [17] with >10 ns laser pulses at or above atmospheric pressure, where breakdown was fully in the avalanche regime.

The single-pulse output of the laser is split, with one beam (E_1) sent to the axicon and the other (E_2), with variable delay, directed to a lens L ($f/10$, $w_0=10$ μm, Rayleigh length $\pi w_0^2/\lambda=300$ μm) and focused from the opposite direction onto the end of the axicon spark. A

beam splitter behind the axicon and a microscope objective (L_2) are used to image the end of the channel onto CCD$_2$ and to measure the coupling efficiency of the lens beam into the channel; see Fig. 3(a). Initial alignment is achieved by monitoring (CCD$_1$) fluorescence and laser scattering as the sparks are generated at 10 Hz. For 30 torr of Xe, $E_1=150$ mJ (peak axicon-focused intensity 4×10^{13} W/cm^2), $E_2=5$-40 mJ, and delay of 15 ns, the axicon spark is strongly and uniformly lit up in fluorescence at best transverse alignment of the lens beam. At this density, the axicon spark is produced mainly by MPI. Lateral deviation of the lens beam by 20 μm in any direction gives rise to enhanced fluorescence only at the leading end, interpreted as interaction with the higher density plasma of the expanding shock. Laser scattering was observed using a mix of 160 torr N$_2$ and 30 torr Xe, with Xe promoting avalanche ionization. Figure 3(b) shows
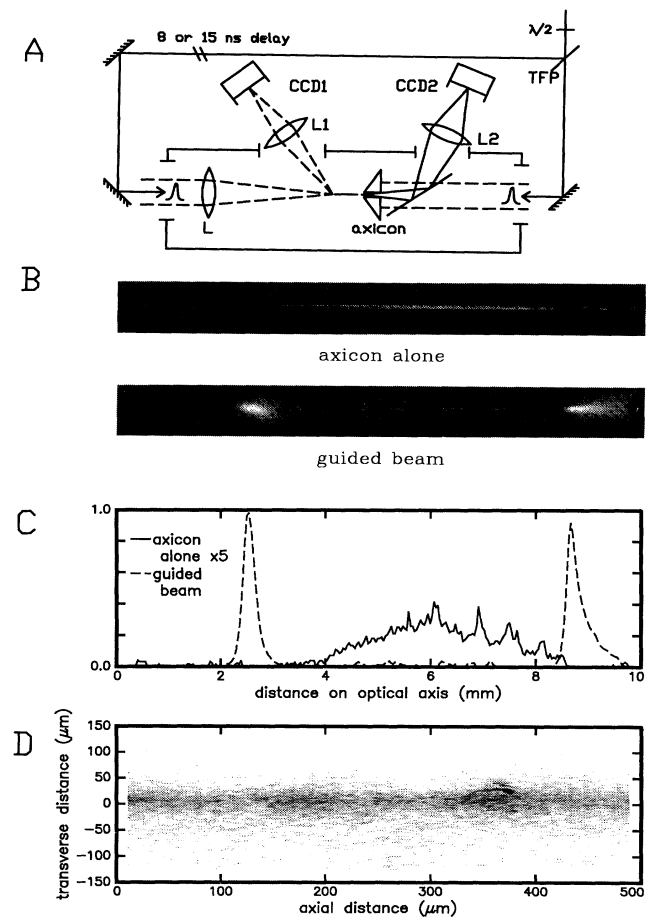

FIG. 3. (a) Optical arrangement for second experiment. (b) Laser scattering images (CCD$_1$) (for $E_1=150$ mJ, $E_2=25$ mJ, delay of 15 ns): (i) axicon alone ($\times$5) and (ii) optimum alignment for guiding of lens beam in channel, showing scattering at channel entrance and exit. Lens L is to the left. (c) Line outs of images in (b). (d) Thomson scattering image of channel section near center. The scattering image width is 35 μm.
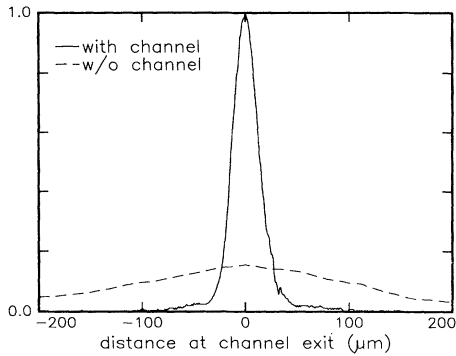
FIG. 4. Line outs of images (CCD_2) from location of channel end with and without channel present; the guided mode is near Gaussian with FWHM $=25$ μm.

that at best alignment of the lens beam, scattering of roughly equal amounts appears at the entrance *and* exit to the axicon spark, with much weaker contribution from the channel; transverse deviations of 20 μm in *any* direction produce scattering only at the entrance. Axial movement of L to focus positions away from the entrance produces an isolated spark whose location jitters axially due to seeding of the local avalanche by electrons or ultraviolet emission from the axicon breakdown. Focusing too far into the channel produces scattering at this focus alone. Decreasing the delay to 8 ns resulted in strong fluorescence and laser scattering at the leading end only. The scattering at the ends [Fig. 3(c)] increases exponentially with lens beam energy above a detection threshold of 5 mJ, an indication of a nonlinear scattering process; below this threshold, guiding is still observed via CCD_2. The end scattering is much less pronounced if Ar is used in place of N_2. The much weaker Thomson scattering from the channel interior was imaged by a microscope objective onto a higher sensitivity CCD camera (in place of CCD_1). The lens beam is polarized at 90° to the axicon beam; its scattering image was filtered with a polarizer. This image, Fig. 3(d), shows a section of channel with a scattering region of width 35 μm. This width extends for the full length of the channel between the end scattering points. At best alignment, we observe with CCD_2 a near-Gaussian mode of FWHM 25 μm at the channel exit, containing 77% of the energy in the vacuum focal spot of lens L (Fig. 4) for $E_2 = 40$ mJ. The image without the channel present is also shown for comparison. For longer delays, or closer-in positions of L, we observe what appear to be higher order modes. As another check for guiding, a variable aperture was placed on the axicon; decreasing the aperture diameter reduces the diameter of the beam transmitted by the axicon, resulting in a shorter channel. With the channel length reduced to 4 mm, the mode image of the end of the channel (CCD_2) is the same size as in Fig. 4.

In effect, at optimum alignment *we observe optical*

guiding *over the 24 Rayleigh lengths of the axicon channel at intensities in the range of 10^{13}-10^{14} W/cm^2*, based on E_2, the coupling efficiency, and the guide mode and channel imaging at various delays. In this intensity range, the channel supports mode structure reminiscent of an optical waveguide.

[1] J. H. Mcleod, J. Opt. Soc. Am. 44, 592 (1954).
[2] J. M. Dawson, A. Hertzberg, R. E. Kidder, G. C. Vlases, H. G. Ahlstrom, and L. C. Steinhauer, in *Plasma Physics and Controlled Nuclear Fusion Research* (IAEA, Vienna, 1971), Vol. I, p. 673.
[3] N. H. Burnett and P. B. Corkum, J. Opt. Soc. Am. B 6, 1195 (1989).
[4] T. Tajima and J. M. Dawson, Phys. Rev. Lett. 43, 267 (1979); P. Sprangle, E. Esarey, A. Ting, and G. Joyce, Appl. Phys. Lett. 53, 2146 (1988).
[5] X. F. Li, A. L'Huillier, M. Feray, L. A. Lompré, and G. Mainfray, Phys. Rev. A 39, 5751 (1989).
[6] For example, A. Sullivan, H. Hamster, H. C. Kapteyn, S. Gordon, W. White, H. Nathel, R. J. Blair, and R. W. Falcone, Opt. Lett. 16, 1406 (1991).
[7] A. B. Borisov et al., Phys. Rev. Lett. 68, 2309 (1992); R. W. Falcone, in *X-Ray Lasers—1992*, edited by E. E. Fill, IOP Conf. Proc. No. 125 (Institute of Physics, London, 1992), p. 213.
[8] P. Sprangle, E. Esarey, J. Krall, and G. Joyce, Phys. Rev. Lett. 69, 2200 (1992).
[9] T. M. Antonsen and P. Mora, Phys. Rev. Lett. 69, 2204 (1992).
[10] P. Monot, T. Auguste, L. A. Lompré, G. Mainfray, and C. Manus, J. Opt. Soc. Am. B 9, 1579 (1992).
[11] P. E. Young, H. A. Baldis, R. P. Drake, E. M. Campbell, and K. G. Estabrook, Phys. Rev. Lett. 61, 2336 (1988).
[12] G. A. Askar'yan and N. M. Tarasova, Pis'ma Zh. Eksp. Teor. Fiz. 20, 277 (1974) [JETP Lett. 20, 123 (1974)].
[13] L. C. Johnson and T. K. Chu, Phys. Rev. Lett. 32, 517 (1974); T. K. Chu and L. C. Johnson, Phys. Fluids 18, 1460 (1975).
[14] M. V. Ammosov, N. B. Delone, and V. P. Krainov, Zh. Eksp. Teor. Fiz. 91, 2008 (1986) [Sov. Phys. JETP 64, 1191 (1986)].
[15] C. G. Durfee III, and H. M. Milchberg, Opt. Lett. 17, 37 (1992).
[16] V. V. Korobkin, L. Ya. Polonsky, V. P. Poponin, and L. N. Pyatnitsky, Kvanti Elektron. 13, 265 (1986) [Sov. J. Quantum Electron. 16, 178 (1986)].
[17] R. Tremblay, Y. D'Astous, G. Roy, and M. Blanchard, Opt. Commun. 28, 193 (1979); F. V. Bunkin, V. V. Korobkin, Yu. A. Kurinyi, L. Ya. Polonsky, and L. N. Pyatnitsky, Kvant. Elektron. 10, 432 (1982) [Sov. J. Quantum Electron. 13, 255 (1983)].
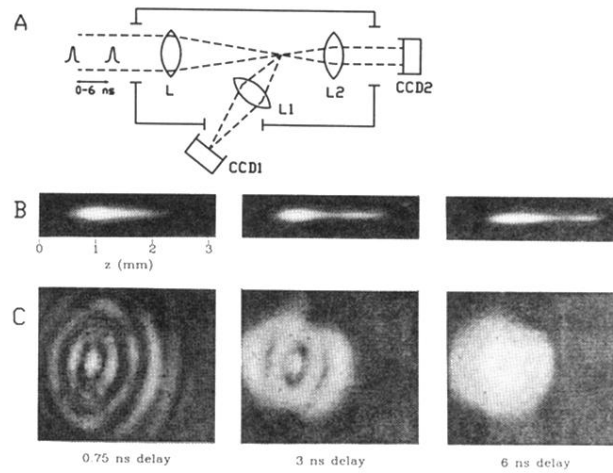
FIG. 2. (a) Optical arrangement for first experiment. (b) Fluorescence images (CCD$_1$) from spark in 30 torr Ar with $E_1 = 70$ mJ, $E_2 = 70$ mJ, and $w_0 = 10$ μm for various delays of pulse 2. Lens L is to the left. (c) Probe (pulse 2) far-field patterns (CCD$_2$) for the same delays as (b).
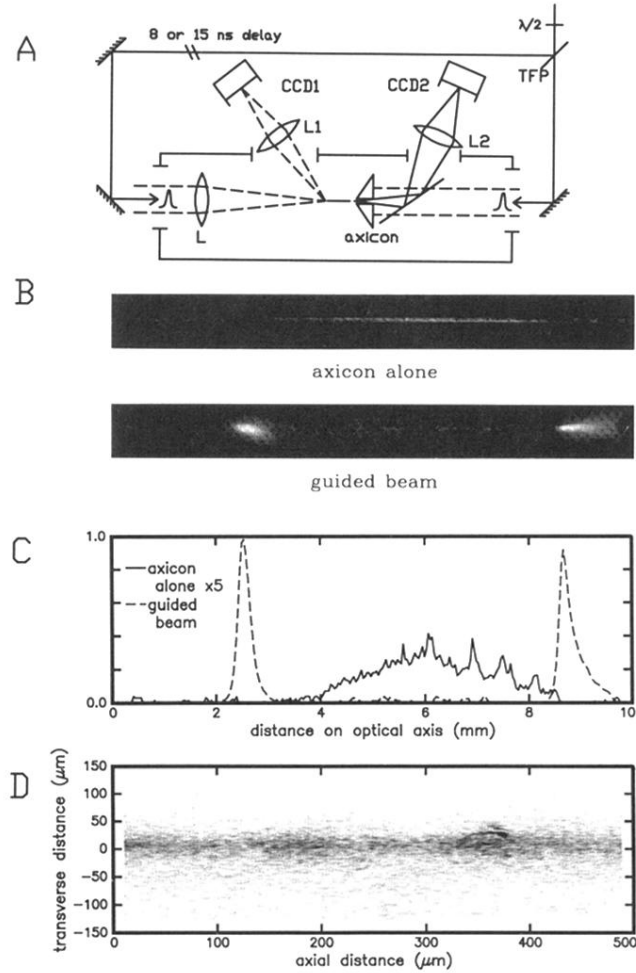
FIG. 3. (a) Optical arrangement for second experiment. (b) Laser scattering images (CCD$_1$) (for $E_1 = 150$ mJ, $E_2 = 25$ mJ, delay of 15 ns): (i) axicon alone ($\times 5$) and (ii) optimum alignment for guiding of lens beam in channel, showing scattering at channel entrance *and* exit. Lens L is to the left. (c) Line outs of images in (b). (d) Thomson scattering image of channel section near center. The scattering image width is 35 μm.